Solar Energy 166 (2018) 171–180

Contents lists available at ScienceDirect

Solar Energy

journal homepage: www.elsevier.com/locate/solener

Development of an electronic load I-V curve tracer to investigate the impact of Harmattan aerosol loading on PV module pern2tkformance in southwest Nigeria

Alexander A. Willoughby*, Muritala O. Osinowo

Department of Physical Sciences, Redeemer's University, Ede, Nigeria

ARTICLE INFO

Keywords:
Photovoltaic module
I-V/P-V characteristics
MOSFET electronic load
I-V curve tracer
Arduino
Aerosol
PV soiling

ABSTRACT

This study investigates the impact of the seasonal Harmattan aerosol loading on PV module efficiency at a station in Southwest Nigeria. To this end, a simple, open-source, cost effective electronic load I-V curve tracer was developed to compare the I-V characteristics of a pair of horizontally positioned 80 W monocrystalline modules for the duration of the Harmattan period. The control module was regularly cleaned manually and the other module left to accumulate the Harmattan dust deposits. In order to obtain the modules' characteristic parameters, an Arduino-based pulse width modulation (*pwm)* duty cycle was implemented to vary simultaneously, the gate-source voltages, V_{GS}, of two power metal-oxide semiconductor field-effect transistors (MOSFETs) acting as fast variable loads for the modules. Experimental results acquired from the prototype circuit demonstrate that this method provides a more accurate approach and faster response than the resistive load tracer method. The prototype instrument was able to measure and reproduce characteristic curves that are obtainable from the more expensive branded products. Resulting curves depict reduction in the short circuit current, I_{SC}, the current at maximum power, I_{MP}, the power output, P_{MP} and the efficiency, η of the dusty module by more than 18% in comparison with the control module over the measurement period.

1. Introduction

Inherent problems associated with PV systems include challenges peculiar to the climate and weather patterns of the locale in which the system is to be installed. Knowledge of weather conditions, particularly solar irradiance, one of the critical input factors required for evaluation of PV power generation, is pertinent for adequate system sizing.

Nigeria is a tropical country situated between 3–14°E of longitude and 4–14°N of latitude and supplied with ample amount of sunlight all year round; it's annual average daily solar radiation is about 5.25 kWh/m^2 per day, varying between 3.5 kWh/m^2 per day at the coastal areas and 7.0 kWh/m^2 per day at the Northern boundary, and an annual average daily sunshine of 6.25 h ranging between 3.5 h at the coastal areas and 9.0 h at the far northern boundary (Abdusalam et al., 2012). During the rainy season from May to October, the atmosphere is mostly cloudy and suffused with large amounts of water vapour, especially in the coastal, eastern and southern regions. The rains begin to recede in late October and soon after, say, middle November, the atmosphere becomes hazy, giving notice of the incoming dry Harmattan season. This is the seasonal southward migration of the dry weather emanating from the Sahara desert between November and March of the following year. It brings along with it the vertical aerosol loading of the atmosphere across the expanse of West Africa. The southward migration of this Harmattan dust front is associated with the migration of the Inter Tropical Discontinuity (ITD) weather system (Ojo, 1977). The ITD (also known as the Inter Tropical Convergence Zone, ITCZ) is the north-south movement of a zone of discontinuity or the boundary between the moist south-westerly, tropical maritime (mT) monsoon air mass originating from the Gulf of Guinea, and the hot, dry north-easterly tropical continental (cT) air mass blowing down from the Sahara Desert. By the end of January to mid February, the ITD holds a position of approximately 6°N and all regions north of this latitude will be under the influence of cT air mass, resulting in dry season conditions across West Africa (Ojo, 1977). Ede (7°44′20″N, 4°26′10″E), the southwest station in Nigeria under study, lies along the path of this front and very much receives both weather conditions. Therefore, between November and March, the Harmattan aerosol dust descends on the whole country. Invariably, solar irradiance reaching down is scattered and diffuse which in turn results in the degradation of PV system performance.

* Corresponding author.
E-mail addresses: lexy_willy@yahoo.com, willoughbya@run.edu.ng (A.A. Willoughby), osinowom@gmail.com (M.O. Osinowo).

https://doi.org/10.1016/j.solener.2018.03.047
Received 11 December 2017; Received in revised form 13 March 2018; Accepted 17 March 2018

1.1. Dust degradation

In designing and sizing backup systems, these weather patterns affecting insolation mentioned above are usually factored into the solar resource assessment otherwise the PV system energy requirement may not be accurately sized and the backup system could turn out to be inefficient. Dust deposition on PV modules is one of the issues hampering efficient performance of modules and has been studied by several authors (Ndiaye et al., 2013; Sulaiman et al., 2011; Kaldellis et al., 2011; Siddiqui and Bajpai, 2012; Mani and Pillai, 2010; Gupta, 2017; Sayyah et al., 2014; Tanesab et al., 2015; Saidan et al., 2016; Paudyal and Shakya, 2016). It was shown from these studies that dust deposition on PV modules caused a significant reduction in efficiency and energy yield of the modules. In urban areas, other aerosols, e.g., suspended particulate matter of different size distributions that can contribute to diminishing the efficiency of a module – soot, ocean spray, carbon monoxide exhaust from poorly maintained vehicles, chemical fallout from factories, all settle on PV modules. These particles possess light (photon) absorbing and scattering coefficients which ultimately contribute, to some degree, the attenuation of the incoming solar radiation and consequently the reduction in output energy of the module (Sayyah et al., 2014; Tanesab et al., 2015; Saidan et al., 2016; Paudyal and Shakya, 2016; Babatunde et al., 2009; Park et al., 2011; Wang et al., 2009).

In Nigeria, visual inspection of solar street lights and mounted roof top PV modules in different cities across the country reveal that they are mostly caked with layers of accumulated dust and grime that have not been cleaned for a long time. Consequently, backup system batteries are usually not adequately charged by either *pwm* or MPPT charge controllers. A common method of assessing the electrical output performance of a PV module is by scanning the current - voltage (I-V) and power - voltage (P-V) characteristics of the module (Ndiaye et al., 2013; Kopp, 2012; Ramaprabha et al., 2015; Leite and Chenlo, 2010; Leite et al., 2012; Kuai and Yuvarajan, 2006). Performance indicators largely affected by dust deposition on modules are the short circuit current, I_{SC}, current at maximum power, I_{MP}, maximum power, P_{MP} and efficiency, η. This work investigates the impact of the 2016/2017 seasonal Harmattan aerosol loading on PV modules in Ede by developing an I-V curve tracer with a power MOSFET acting as the load. Characteristic curves of two modules, one the clean (control) module and the other with dust accumulation on it are then compared in order to observe the effect of dust on PV performance. The work is also an improvement on the resistive load I-V curve tracer presented in a previous work (Willoughby et al., 2014).

1.2. I-V curve tracers

Apart from measuring I-V characteristics, curve tracers are also fast functional instruments for checking observable signs of module performance, defects, weathering and degradation. In recent past, several studies have investigated the effect of dust, soiling, shading and weather on PV efficiency and degradation using different kinds of devices (Ndiaye et al., 2013; Hamdaoui et al., 2009; Kopp, 2012). Obtaining accurate results is best achieved by scanning the module characteristics using I-V curve tracers. PV I-V characteristics are typically obtained by varying a load across the module. Different designs of I-V curve tracers abound in literature and are commercially available. A detailed comparison of six different procedures of the designs of I-V curve tracers that have been reported in literature is reviewed by Durán et al. (2008). A number of commercially available I-V curve tracers are available to PV manufacturers, system integrators, contractors and installers with prices dependent on the levels of sophistication, durability, and performance (Renewable Energy Innovation). Ndiaye et al. (2013), investigated the effect of dust on PV module I-V/P-V characteristics in the Sahelian desert environment after a year of exposure of mono- and poly crystalline modules without cleaning. The "I-V 400" instrument used is a hand held PV tester suitable for ordinary and scheduled maintenance of PV systems. It also features temperature and radiation measurement capabilities. From their measurements, they deduced a maximum power output loss from 18% to 78% and 23% to 80% for the poly- and mono crystalline modules respectively.

Due to the prohibitive cost of a branded tracer, a simple, minimalist, cost effective instrument with available off-the-shelf components was designed for the present purpose and for future related experiments by taking advantage of the Arduino open source platform with a view to future design upgrades with more features.

One of the designs enumerated in Renewable Energy Innovation, describes a variable resistive load which seems to be the cheapest and easiest tracer method to implement. In Willoughby et al. (2014), a resistive load type was implemented that comprised of rapidly varying resistive loads centred on power resistors connected to relays and controlled by an electronic circuitry. A 555 astable oscillator transmitted clock pulses to the clock terminal of a 4017 decade counter which in turn produced a sequence of pulses that successively turned on relays via driver transistors. The I-V characteristic points of the module were measured accordingly by the consecutive selection of the relays which were each connected to a selected load resistor to determine the operating point on the I-V curve as seen in Fig. 1(a) and (b). A Pace XR5 eight channel data logger was connected to record the currents and voltages as well as the irradiance. This method of selection of load resistors via relays has its shortcomings, not

(a)

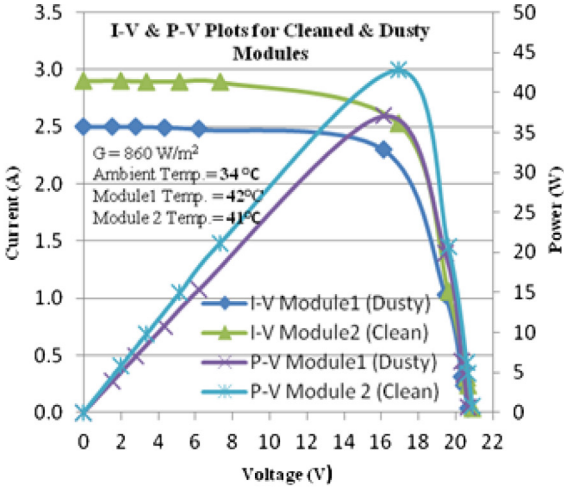

(b)

Fig. 1. (a) Photo of resistive load tracer from previous work, (b) I-V & P-V plots obtained.

least of which is its slow response, de-bouncing of the relay contacts and limited number of load resistors which were inadequate in tracing many points on the plot. Due to these drawbacks, the points on the graph were not smoothly traced. A more accurate and fast measuring equipment was therefore required. From reported literature, a preference for the electronic load type is common, in which a MOSFET is used as a fast variable load (Leite and Chenlo, 2010; Leite et al., 2012; Garrigós and Blanes, 2005; Kuai and Yuvarajan, 2006; Panwar and Mandliya, 2016; Papageorgasa et al., 2015; van Dyk et al., 2002; Zimmerman and Edoff, 2012; Hemza et al., 2015). Generally, in these designs a power MOSFET or an insulated-gate bipolar transistor (IGBT) operates in its linear and active region as a fast varying dc load to trace PV module I-V characteristics.

2. MOSFET as an electronic load

The MOSFET performs as an electronically controlled load that moves the operating point of the PV module over the whole range of I-V curve. When a drive voltage is applied to its gate, it generates a rapid and accurate PV output current from 0 to *Isc* (A) and an output voltage from *Voc* to 0 (V). The rapidity of the scan is made as fast as possible so as to reduce the effect of insolation and temperature fluctuations due to cloud movement or other weather changes (Papageorgasa et al., 2015). In this way, all the points traced on the I-V curve are captured under the same weather conditions in a very short time. The rapid scanning also prevents the MOSFET from overheating (Durán et al., 2008). A basic circuit with a MOSFET as an electronic load is shown in Fig. 2.

From Fig. 2, for an n-channel switching MOSFET with a ground-referenced gate drive, the equations describing its performance are based on the relationship between V_{GS}, and V_{DS}. In Fig. 2, V_{GS}, V_{DS} and I_D are the gate-source voltage, the drain-source voltage and the drain current of the MOSFET respectively; R_S is the current sense resistor connected to ground from the MOSFET source. I_{PV} and V_{PV} represent the current and voltage across the module. The characteristics are expressed as (Kuai and Yuvarajan, 2006):

$$I_D = K(V_{GS}-V_{th})^2 \tag{1}$$

$$= K[2(V_{GS}-V_{th})V_{DS}-V_{DS}^2] \tag{2}$$

where K is the device constant and V_{th} is the gate threshold voltage and Eqs. (1) and (2) represent the constant current and ohmic regions respectively.

The three regimes of operation depicting the relationship between I_D as a function of V_{GS} and V_{DS} are:

(i) Cut-off (MOSFET is OFF):

$$\boldsymbol{I_D} = 0, \text{ if } V_{GS} < V_{th} \tag{3a}$$

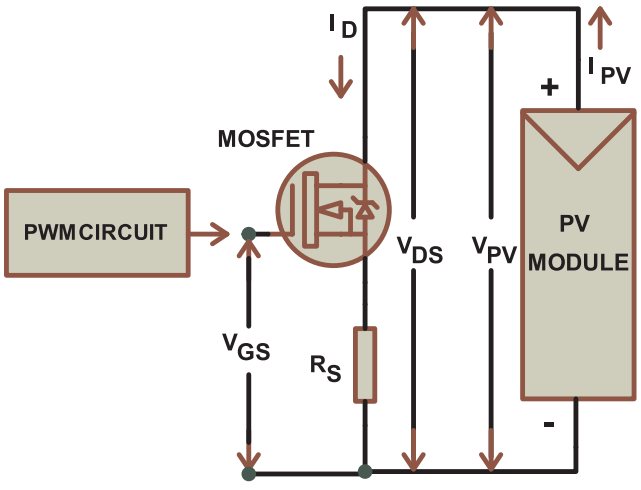

Fig. 2. Basic I-V curve tracer circuit model using MOSFET as an electronic load.

(ii) Ohmic or triode:

$$\boldsymbol{I_D} = \boldsymbol{K}[2(\boldsymbol{V_{GS}}-\boldsymbol{V_{th}})\boldsymbol{V_{DS}}-\boldsymbol{V_{DS}^2}] \text{ if } V_{GS}-V_{th} > 0 \ \& \ V_{DS} < V_{GS}-V_{th} \tag{3b}$$

(iii) Active or saturation:

$$\boldsymbol{I_D} = \boldsymbol{K}(\boldsymbol{V_{GS}}-\boldsymbol{V_{th}})^2 \text{ if } V_{GS}-V_{th} > 0 \ \& \ V_{DS} > V_{GS}-V_{th} \tag{3c}$$

In Eq. (3b), I_D is dependent on both V_{GS} and V_{DS} while in Eq. (3c), I_D depends approximately on V_{GS} only. For a PV module, the output voltage and output current are represented by V_{PV} and I_{PV} respectively.

$$I_D = I_{PV} = I_L - I_{diode} \tag{4}$$

where I_L is the light generated current ($=I_{SC}$) and I_{diode} the ideal diode law:

$$I_{diode} = I_o exp\left[\frac{V_{PV}}{nV_T}-1\right] \tag{5}$$

n = diode ideality factor and V_T the thermal voltage.

Fig. 3 shows a plot in which the module characteristics are super-imposed on the MOSFET characteristics (Leite and Chenlo, 2010; Leite et al., 2012). This is achieved by sweeping the V_{GS} with a *pwm* signal so that the operating point of the MOSFET sweeps the I_{PV} - V_{PV} module characteristic between V_{OC} andI_{SC}. Comparing the module and MOSFET equations, i.e.,

$$V_{PV} = V_{DS} + I_D R_D \tag{6}$$

Combining Eqs. (4) and (6) thus determines the load curve. As current flows, I_{PV} thus develops into I_D. When V_{GS} is increased above V_{th}, the device will operate in its active region where I_D rises approximately linearly with V_{GS}. Accordingly, the operating point is moved up the I-V curve, at the same time corresponding to the intersection of the PV module characteristic with that of the MOSFET's for a given V_{GS}, (Leite and Chenlo, 2010; Leite et al., 2012). Put simply, sweeping V_{GS} from 0 V to 5 V changes the MOSFET's operating point (I_D - V_{DS} characteristics) as well as changing the operating point of the PV module to move along its I_{PV} - V_{PV} characteristic curve.

3. Circuit details of the electronic load tracer

The block diagram of the tracer is shown in Fig. 4. It depicts the Arduino Uno *pwm* signal input, opto-isolator, low pass filter, gate drive amplifier and the MOSFET load. Measured *Isc* and *Voc* are fed into the Pace XR5 data logger via op amps.

3.1. The Arduino as PWM driver

The Arduino platform comprises the hardware and the software sections which form the basic structure of the device. The code for the software is relatively simple and tutorials can be obtained from the Arduino website (http://www.arduino.cc).

To provide *pwm* gate drive voltage, V_{GS} for the MOSFET load, the authors Leite and Chenlo (2010), Leite et al. (2012) and Kuai and Yuvarajan (2006) combined discrete circuits comprising sine and saw-tooth waveform generators and a mixing amplifier. The circuit implementation is much simplified and advantageous using the Arduino's embedded *pwm* generator. At the press of a button, *pwm* can be generated and its duty cycle and speed controlled by code. Kopp (2012), Panwar and Mandliya (2016), Papageorgasa et al. (2015), Hemza et al. (2015) and Renewable Energy Innovation built their circuit based on the Arduino platform. Using the Arduino affords the feature to also display results on a screen. In Renewable Energy Innovation, the I-V curve tracer was based on the Arduino platform with an additional LCD display feature that displays essential parameters like P_{MP}, V_{OC} and I_{MP}. The output is streamed via a serial connection and can be recorded on a computer. Designs by Papageorgasa et al. (2015) and Hemza et al. (2015), were based on an open-source Arduino compatible platform that was used for controlling the

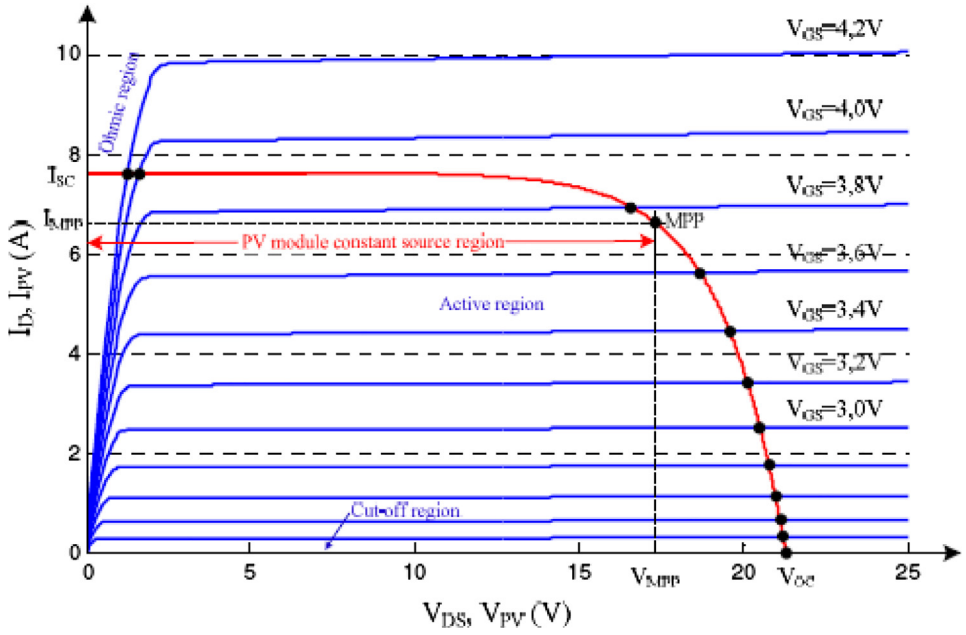

Fig. 3. Characteristic of a PV module at STC (red curve) and characteristics of a MOSFET (blue curves). (For interpretation of the references to colour in this figure legend, the reader is referred to the web version of this article.) Plot reproduced from (Leite and Chenlo, 2010; Leite et al., 2012).

electronic load as well as measuring the current and voltage of the panel. Hemza et al. (2015), based their I-V curve tracing on the National Instrument's LabVIEW Interface for Arduino (LIFA) toolkit. The toolkit can control or acquire data from the Arduino microcontroller. The open source Arduino was used to control a MOSFET load as well as acquire the current and voltage values from the test panel, which were then transferred to a supervisory computer.

3.2. The full I-V curve tracer circuit

The full circuit of the tracer is shown in Fig. 5. The Figure shows the circuit designed to trace the curves for one module (i.e., *clean module*). The circuit was duplicated to trace the curves of the dusty module. Select pins 3 and 11 on the Arduino use its analogWrite() command to generate the *pwm* signals to drive the gate of the MOSFETs. The I-V curve can be measured in both directions, from short-circuit current, I_{SC} to open-circuit voltage V_{OC} and vice versa, the time in seconds dictated by input to the code. A double loop structure in the code increases each pin's output from 0 to 5 V and then decreases it from 5 V to 0 V. A portion of the Arduino code can be found in Appendix A.

The Arduino *pwm* pins 3 and 11 are configured to put out 488 Hz, using the analogWrite function. Its duty cycle signal is varied from 0 V to 5 V, i.e., from 0% to 100% or 0–255 ADC, at the press of a push button. By varying the Arduino's output to the MOSFETs' gates, the operating point of the MOSFET automatically scans a module's I-V characteristic curve between the short circuit current and open circuit voltage points. Consequently, the module characteristic parameters: I_{SC}, V_{OC}, I_{MP}, V_{MP} and P_{MP} are then obtained. LED 1 is observed to increase in brightness during this process. In the reverse direction, it is seen to fade. The speed of the scan is determined by the value assigned to the delay parameter, *d*, in the code. At the discretion of the operator, *d* can be varied from 2 to 5 s. The *pwm* signal is fed into a 4N35 opto-isolator, U1, which provides isolation and protection of the Arduino. The emerging signal from U1 is amplified by an (1× gain) inverting

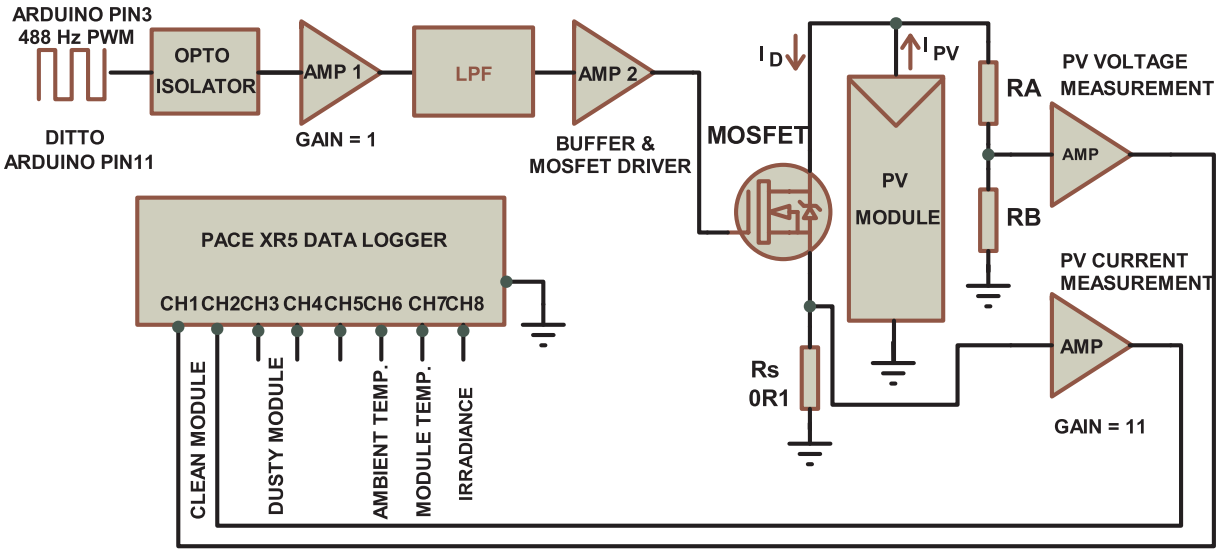

Fig. 4. Block diagram of circuit setup.

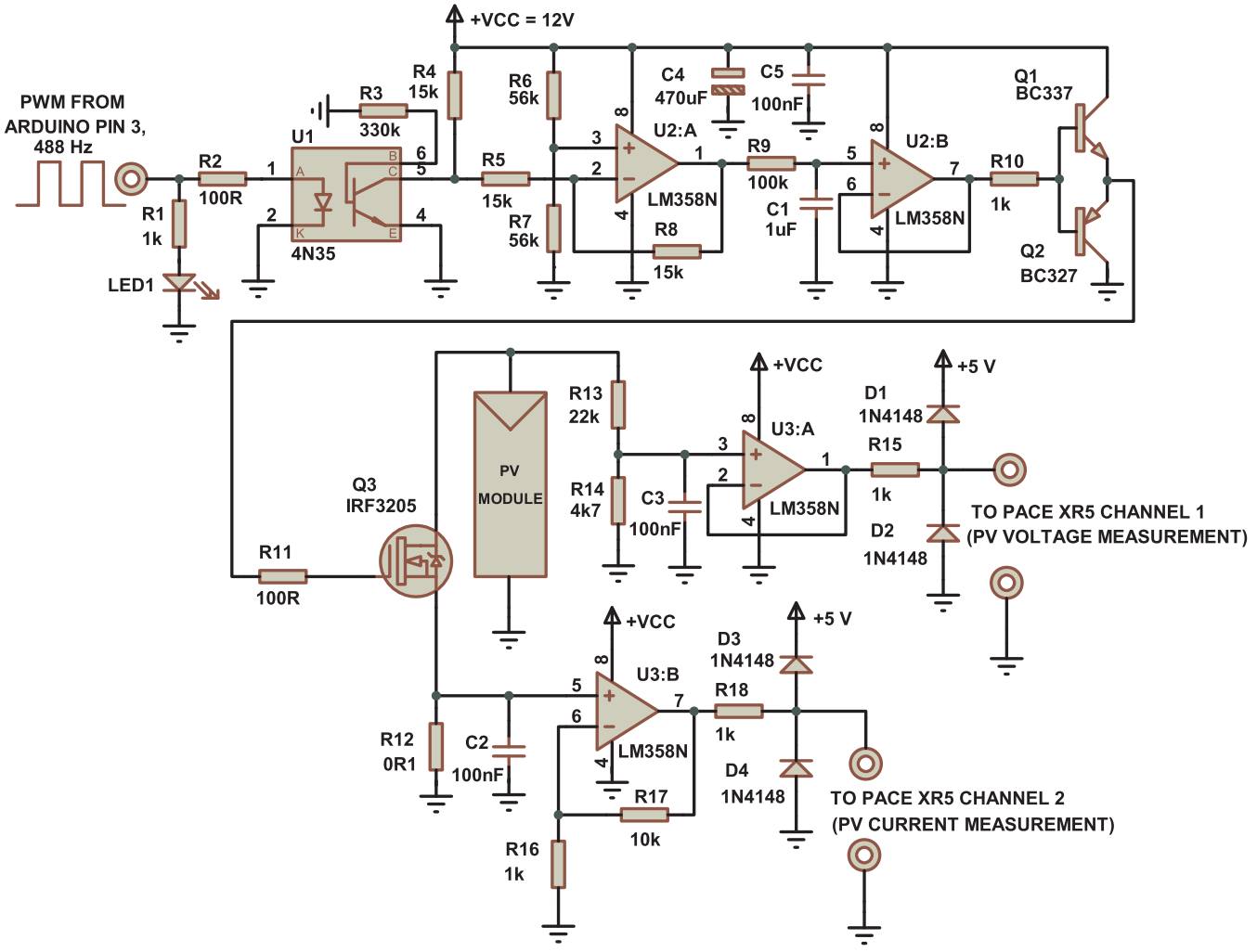

Fig. 5. The full circuit of the I-V curve tracer showing the IRF3205 MOSFET load.

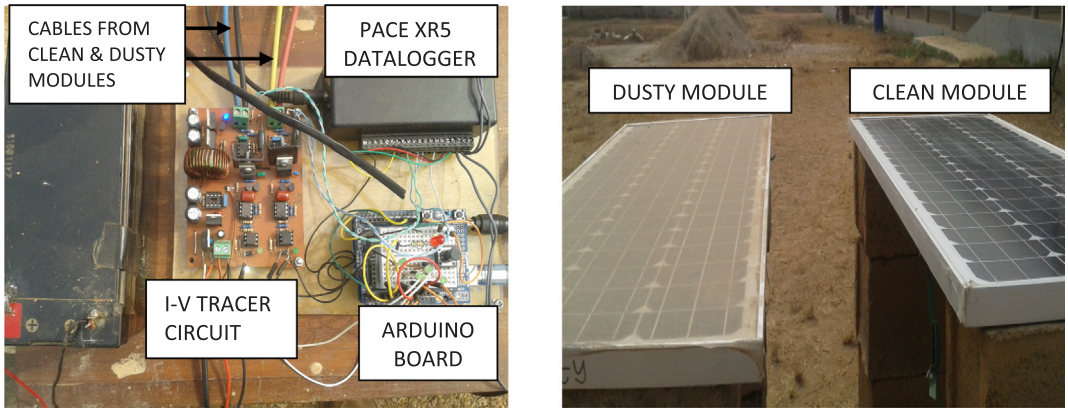

Fig. 6. (a) The circuit set up. (b) The clean and dusty modules.

amplifier, U2:A, one section of an LM358 dual op amp. The response time of the 4N35 to higher frequencies is slow; hence the choice for the value of 488 Hz output frequency. A single pole low pass filter, LPF, formed by R9 and C1, smoothes and converts the signal from U2:A to a dc voltage which is further buffered by a voltage follower, U2:B and the totem pole transistor pair BC337/BC327, driving the gate of the IRF3205 MOSFET. To ensure a smooth output, the RC constant of the filter (i.e. $\tau = RC = 100\,k\Omega \times 1\,\mu F = 100\,ms$) is required to be greater than the Arduino's *pwm* duty cycle ($\tau = 1/488\,Hz = 2\,ms$). Resistors R10 and R18 reduce high currents that may appear at the input channels of the Pace XR5 data logger. C2 and C3 trim down high voltage pulse transients as well as providing some filtering. Clamp diodes D1–D4 provide extra protection and ensure that any high voltage that may be applied to the input of the XR5 is always clamped at 5 V. The setup as well as the conditions of the modules is illustrated in Fig. 6 below. Power to the circuit is provided by a 12 V, 7 Ah battery and a

7805 voltage regulator tapped from this source to provide 5 V to the cathodes of clamp diodes D1 and D3.

4. Experimental procedure

4.1. PV voltage measurement and logging

Both modules were positioned horizontally, about five feet off the ground in an open, obstruction free environment where they were directly exposed to dust deposition. The location was at the Department of Physics & Electronics, Redeemer's University, Ede, Osun state, Nigeria. While the control module was manually cleaned at two days intervals with water using a wet towel and dried, the other module was left untouched and dust allowed to build up on it. Each panel was connected to one input of the I-V curve tracer circuit board. The voltages and currents obtained from the clean module were connected to the input channels 1 and 2 of a Pace XR5 data logger respectively. Similarly, the voltages and currents from the dusty module were connected to input channels 3 and 4 respectively. Channels 6, 7 and 8 were used to log ambient temperature, module backside temperature and irradiance respectively. These two parameters were measured with the PT907 temperature probes and the SRS-100 solar radiation sensor, both provided by Pace Scientific Inc. The PT907 is recommended for monitoring temperature range of −40 to 105 °C and has an accuracy of ± 0.15 °C, while the SRS-100 has a measurement range of 0–1500 Wm^{-2} and accuracy of ± 5%. The SRS-100 is positioned in the plane of the clean module. By pressing the switch button on the Arduino board, the circuit automatically scanned both modules simultaneously and data transferred to memory of the logger.

The Pace XR5 is a standalone data logger with 8 multirange analog inputs that sensors can be connected to directly. Logged data can be transferred to a pc/laptop for graphing and analysis, i.e., transferred data is formatted and opened as a readable, Excel compatible text file with extension ".txt". The maximum input voltage that the Pace XR5 data logger can accommodate is 5 V. In order to be able to log voltages as high as 22 V from the PV module, without exceeding the maximum requirement input of the XR5, the output voltages of the panels were dropped using the potential divider consisting of R_A and R_B (R13 and R14 in Fig. 5) whose function is to scale down the PV voltage from 22 V to ≤5 V. With the values shown in the circuit for R13 and R14, the maximum scaled down voltage input into channel 1 of the XR5 for the 'control' panel is calculated as given in Appendix B. The voltage is buffered by a voltage follower U3:A before being fed into channel 1 of the logger. The same set of resistors is replicated for the 'dusty' channel 3. Therefore, the actual PV voltage that will be calculated and read from the logger is as given in Appendix B.

4.2. PV current measurement

In Renewable Energy Innovation, current was measured via a 0.005 O shunt resistor and AD8211 high-side current sense IC was used to convert this small voltage into a current reading for the microcontroller. In this work, current measurement is tapped off the current sensing source resistor R_S in a low side current sensing configuration. The voltage developed across, $R_S = 0.1\ \Omega$ is amplified by the (11× gain) non-inverting amplifier LM358, U3:B. Retrieval of values of current can be found in Appendix B.

5. Experimental results

The complete arrival of the Harmattan season in the southwest region of the country is usually experienced about early December. As the rains retreat, the ITD pushes south and the dust haze bears down on the region. Although the turbidity of the atmosphere is gradually increasing, no appreciable dust is deposited at this time. By the end of December, the Harmattan season has intensified and the dust thickness on a PV module becomes sizeable enough to cause approximately 100 mA reduction in I_{SC} within an interval of a few days. Measurement of the I-V characteristics for the clean and dusty modules began in early January and ended about mid-March at the conclusion of the dry season. During this period, data were collected when the sun would be directly overhead between 13:00 and 14:00 local time at three to five day intervals. By that time, the region would be experiencing intermittent but short spells of precipitation brought about by radiative heating and cooling. These short term precipitation events have the effect of removing dust from the atmosphere, consequently disrupting the logging process. In addition, the north-south movement of the ITD has reversed its direction and begun pushing in a south-north direction, followed by the moist mT air.

5.1. Module performance indicators

The PV module technical specifications and performance indicators are given below:

At standard test conditions (STC), where global irradiance, G = 1000 W/m^2, module temperature, T = 25 °C, and relative air mass, AM = 1.5

- Power = 80 W ± 5%
- $I_{MP} = 4.45$ A
- $V_{MP} = 18$ V
- $I_{SC} = 4.95$ A
- $V_{OC} = 21.5$ V
- Dim: 116 × 47.5 × 30 cm

(i) *Efficiency:* The irradiance and temperature dependent efficiency η of the module is the ratio of the maximum power delivered by the module to the power of the incident radiation on the module, i.e.,

$$\eta = \frac{P_{MP}}{A \times G} = \frac{I_{MP} \times V_{MP}}{A \times G} = \frac{FF \times V_{OC} \times I_{SC}}{A \times G} \times 100\% \quad (7)$$

where I_{MP} and V_{MP} are the current and voltage at maximum power respectively, A is the surface area of the module and G the irradiance in Wm^{-2}. Therefore the percentage decrease in efficiency due to soiling is expressed as

$$\eta_{decrease} = \frac{\eta_{Clean} - \eta_{Dusty}}{\eta_{Clean}} \times 100\% \quad (8)$$

(ii) *Fill Factor:* The fill factor describes the quality of the PV module based on the "squareness" of the PV curve. Generally between 0.5 and 0.85, the FF is defined by the quotient of maximum power, P_{MP}, and the theoretical maximum power obtained from the product of open circuit voltage and short circuit current, i.e.,

$$FF = \frac{V_{MP} \times I_{MP}}{V_{OC} \times I_{SC}} = \frac{P_{MP}}{V_{OC} \times I_{SC}} \quad (9)$$

5.2. I-V and P-V characteristics

Fig. 7a–d shows typical plots of the prototype tracer's I-V and P-V output curves for the clean and dusty modules for different days progressing from January to March. The difference between the performances and the effect of dust deposits is discernible from the curves where the dusty module exhibits a reduction in each of the parameters: I_{SC}, I_{MP}, P_{MP} and η, in comparison to the clean module. This is to be expected as the dust acts as disperser and attenuator to the incoming solar radiation resulting in less photocurrent being generated by the dusty module.

International Rectifier (IR) datasheet on the fast switching HEXFET IRF3205 power MOSFET lists the following parameters: $I_D = 110$ A, R_{DS} (on) = 8 mΩ, $V_{DSS} = 55$ V, $V_{GS} = \pm 20$ V, $T_J = -55$ to 175 °C. When fully driven, the MOSFET does not completely attain or cut either the

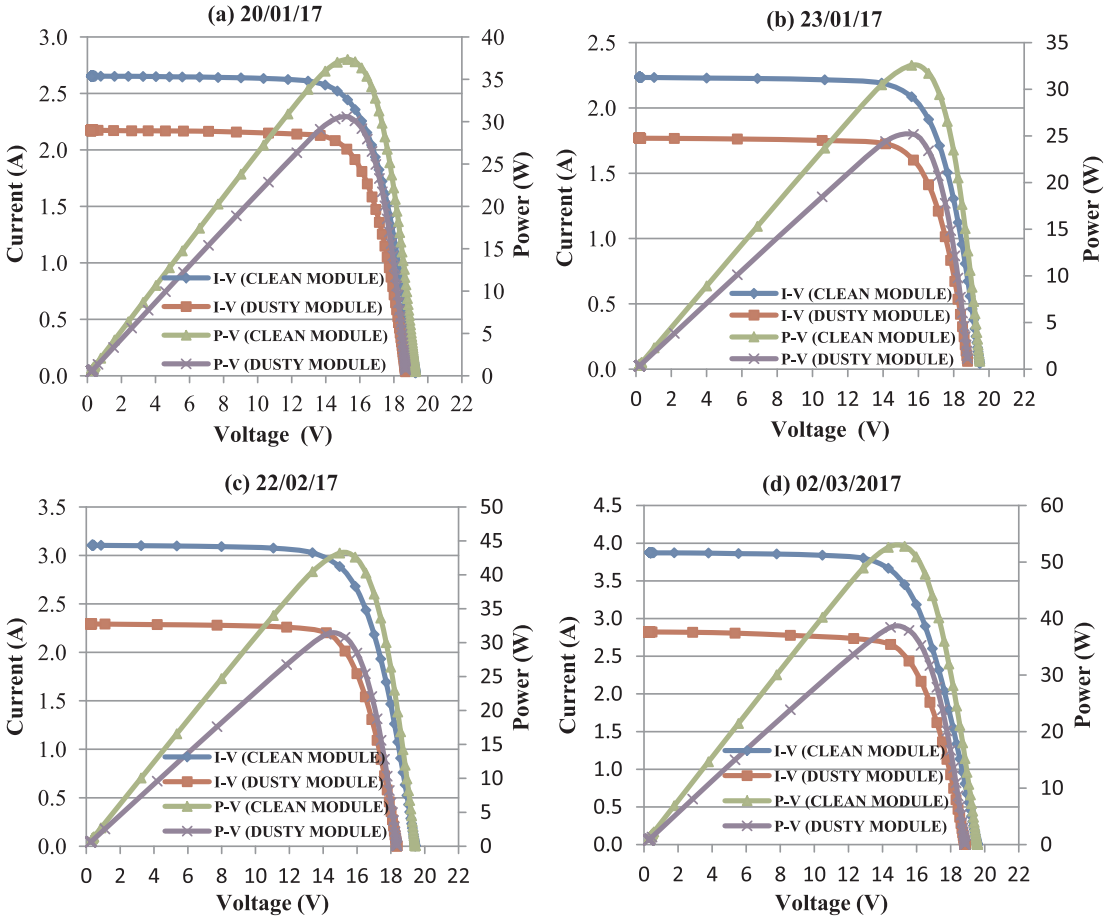

Fig. 7. (a–d) I-V & P-V characteristics of the module logged by the XR5 data logger from the tracer circuit.

maximum open circuit voltage on the V_{OC} axis or maximum short circuit current on the I_{SC} axis. This is because of the contribution of the combination resistance of the MOSFET's drain-source resistance, R_{DS} and the 0.1 Ω current sensing resistor at its source, i.e., ($R_{DS} + R_S$ = 8 mΩ + 0.1 Ω = 108 mΩ). In one of the resulting plots, it was observed that V_{OC} = 0.27 V when I_{SC} = 3.31 A and V_{OC} = 19.96 V when I_{SC} = 0.0033 A. Shunt resistor R_S of 0.005–0.01 Ω and a MOSFET with R_{DS} < 8 mΩ (or paralleling two MOSFETS to reduce the ON resistance) would improve the tracing limits by moving the points much closer to the axes. As these low value shunt resistors were not readily available, 0.1 Ω resistors were subsequently used. A multimeter reading of I_{SC} and V_{OC} obtained by direct measurement before the tracer reading showed that the values were approximately close to the values measured by the tracer. Deviations of not more than 1% drop from the multimeter reading were observed. In Table 1, module underside temperature, $t_{MOD,}$ was observed to vary from 43.6 °C to about 49 °C. The approximately 70% to over 90% rise in module temperature from t_{STC} = 25 °C may also have contributed to the slight drop in voltage from the manufacturer's V_{OC} specification of 21.5 V.

A summary of the results is also shown in Table 1. These also include irradiance measurements G and ambient temperature, t_{AMB}. Relative percentage decreases in these parameters have also been deduced as $\Delta P/P_c$ (%) where ΔP is the difference in parameter between the clean (P_c) and dusty module (P_d). As seen from Table 1, in contrast to the above four parameters, the effect of dust on either the open circuit voltage, V_{OC} or the fill factor, FF is negligible. The relative percentage decrease of V_{OC} range from 3% to 5.5%, while those of FF, vary from 1.3% to 2.8%. This corroborates the results of Ndiaye et al. (2013) and Tanesab et al. (2015) where they asserted that V_{OC} and FF are less sensitive to dust accumulation while short circuit current, I_{SC} and maximum power, P_{MP} are parameters significantly affected by dust deposition. For the period of study, reduction in I_{SC} was observed to vary from 18% to 27%, while currents at maximum power, I_{MP}, varied from 18% to 23%. Maximum power points, P_{MP} show a range above 20–27%. Decreases in efficiencies, η are also affected and range from 20% to 27%.

Fig. 8(a) and (b) shows the curves logged for the control module on 02/03/2017. Just before wiping the preceding five days deposit off the control module, the I-V data were obtained and then immediately logged after cleaning. Meanwhile, the dusty module remained not cleaned. Observation and analysis of the control module show that within a span of five days after the module was cleaned, a deposit of dust caused an equivalent reduction of approximately 160 mA in I_{SC} and I_{MP} and about 3 W in P_{MP} at irradiance level of approximately 800 Wm^{-2}.

6. Conclusions

A simple, open-source, and cost effective electronic load I-V curve tracer has been developed to study the seasonal impact of Harmattan dust and aerosol loading on the output performance of a monocrystalline PV module in southwest Nigeria. By implementing its analogWrite function, an Arduino Uno's pulse-width modulation (*pwm*) duty cycle was used to simultaneously control the gate-source drive voltage of two power MOSFETs acting as electronic fast variable loads. The MOSFET load moves the operating point of each PV module over the whole I-V curve. Experimental results demonstrate that the device is able to generate I-V curves showing a clear distinction between output characteristics of a regularly cleaned PV module compared to one that has accumulated Harmattan dust and aerosols over a period of time. From the plots of I-V and P-V characteristics generated and logged, differences in performance parameters such as short circuit current, I_{SC},

Table 1
Comparison of the electrical output characteristics of the clean and dusty modules.

Date/Irradiance/Temperature	Parameter, P	Clean Module, P_C	Dusty Module, P_d	$\Delta P = P_C - P_d$	Rel. percent reduction $\Delta P/P_c$ (%)
20/01/2017	I_{SC}	2.65	2.17	0.48	18.1
	V_{OC}	19.27	18.69	0.58	3.0
$G = 560\ Wm^{-2}$	I_{MP}	2.44	2.01	0.44	17.8
$t_{AMB} = 36\ ^\circ C$	V_{MP}	15.28	15.24	0.048	0.3
$t_{MOD} = 44\ ^\circ C$	P_{MP}	37.36	30.59	6.77	18.1
	η	0.12	0.09	0.022	18.2
	FF	0.73	0.75	0.03	2.7
27/01/2017	I_{SC}	2.82	2.26	0.56	19.9
	V_{OC}	19.44	18.81	0.63	3.2
$G = 590\ Wm^{-2}$	I_{MP}	2.59	2.10	0.48	18.6
$t_{AMB} = 42.8\ ^\circ C$	V_{MP}	15.56	15.12	0.44	2.8
$t_{MOD} = 43.6\ ^\circ C$	P_{MP}	40.22	31.82	8.41	20.9
	η	0.12	0.09	0.03	23.0
	FF	0.73	0.74	0.01	1.3
22/02/2017	I_{SC}	3.11	2.29	0.82	26.4
	V_{OC}	19.43	18.35	1.08	5.5
$G = 620\ Wm^{-2}$	I_{MP}	2.89	2.20	0.69	23.9
$t_{AMB} = 43.9\ ^\circ C$	V_{MP}	14.97	14.18	0.79	5.3
$t_{MOD} = 48.9\ ^\circ C$	P_{MP}	43.21	31.23	11.98	27.7
	η	0.13	0.09	0.04	27.7
	FF	0.72	0.74	0.02	2.8
02/03/2017	I_{SC}	3.88	2.82	1.06	27.3
	V_{OC}	19.56	18.84	0.72	3.7
$G = 800\ Wm^{-2}$	I_{MP}	3.45	2.66	0.79	22.9
$t_{AMB} = 44.6\ ^\circ C$	V_{MP}	15.30	14.47	0.83	5.4
$t_{MOD} = 47.9\ ^\circ C$	P_{MP}	52.77	38.49	14.33	27.2
	η	0.12	0.08	0.03	33.3
	FF	0.70	0.72	0.02	2.9

$G \rightarrow$ Irradiance, $t_{AMB} \rightarrow$ Ambient temperature, $t_{MOD} \rightarrow$ Clean module underside temperature.

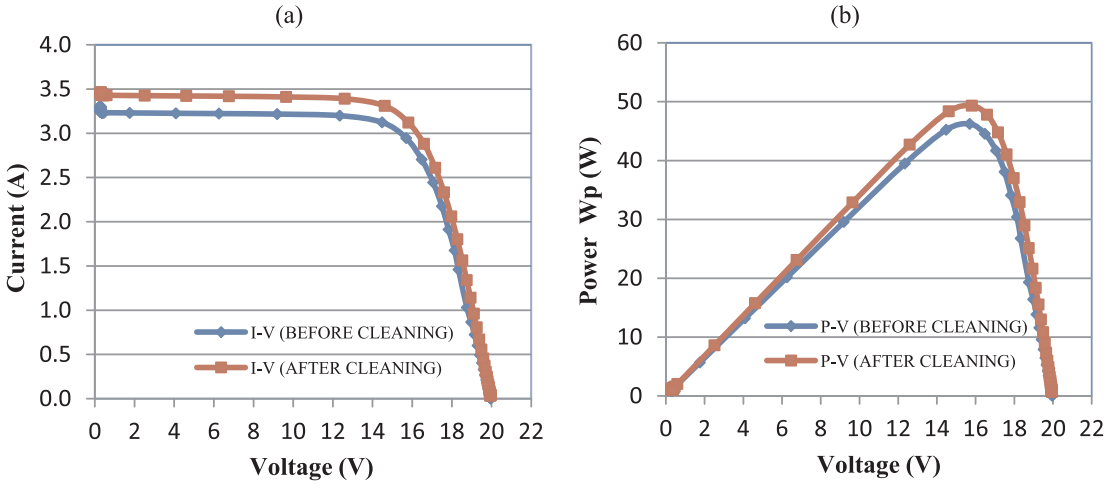

Fig. 8. (a) I-V & (b) P-V characteristics of the control module on 02/03/2017 showing level of accumulation of dust five days after the previous recording of the tracer.

current at maximum power, I_{MP}, maximum power, P_{MP} and efficiency, η, between the two cases are clearly discernible. Values of greater than 18% reduction in these parameters have been observed. Some advantages of this instrument over the resistive load type include its simplicity, cost-effectiveness, readily available open-source components and the rapidity of the scan to capture many more points on the I-V curve in a very short time. The prototype instrument is able to measure and reproduce smooth characteristic curves that are equally obtainable from the more expensive branded products and therefore offers a workable alternative to commercial grade tracers. It is a low-cost testbed instrument that is replicable and can be used by the scientific community for experiments in PV I-V curve tracing. The proposed circuit may be further developed to form the basis of much more sophisticated measuring instrument by including add - on functions such as module string measurement, radiation and temperature measuring algorithms as well as a display meter. The data logging features of Arduino can also be implemented to replace the Pace XR5 standalone logger. Analyses in field test conditions, identification of PV degradation and malfunction conditions are also possibilities that are achievable.

Funding

This research work did not receive any specific grant from funding agencies in the public, commercial, or not-for-profit sectors.

Appendix A. Appendix A

A.1. Arduino code snippet

```
int d = 10;
int switchStatus = LOW;
int stateButton;
const int BUTTON = 2;
const int FAN = 4;
const int MONOCLEAN = 3;
const int MONODUSTY = 11;

void setup(){
  TCCR2B = TCCR2B & 0b11111000 | 0 × 04;   // Setting divisor frequency to 488 Hz from pins 3 & 11
  Serial.begin(9600);
  pinMode (BUTTON, INPUT);
  pinMode (FAN, OUTPUT);
  digitalWrite(FAN, LOW);

  pinMode (MONOCLEAN, OUTPUT);
  digitalWrite(MONOCLEAN, LOW);
  pinMode(MONODUSTY, OUTPUT);
  digitalWrite(MONODUSTY, LOW);
  }

void loop() {
  int stateButton = digitalRead(BUTTON);
  if (stateButton = = 1)   // if button is pressed
    {
      digitalWrite(FAN, HIGH);
      for (int i = 0; i < 255; i + + )   // From 0 to 5 V
        {
          analogWrite(MONOCLEAN, i);
          analogWrite(MONODUSTY, i);
          delay(d);
        }
      delay(5 0 0);
      for (int i = 255; i > 0; i–)   // From 5 V to 0
    {
    analogWrite(MONOCLEAN, i);
    analogWrite(MONODUSTY, i);
    delay(d);
    }
    delay(50);
  }
```

Appendix B. Appendix B

B.2. PV voltage measurement

$$V_{CH1} = \left[\frac{R_B}{R_A + R_B}\right] * V_{PV}, i.\ e.\ , \left[\frac{4k7}{22k + 4k7}\right] * 22\ \text{V} = 3.87\ \text{V} \tag{B.1}$$

$$V_{PV} = \left(\frac{4k7}{22k + 4k7}\right)^{-1} * V_{CH1} = 5.68 * V_{CH1} \tag{B.2}$$

In the XR5 software, 5.68 is the scaling factor or slope.

B.2. PV current measurement

The output from U3:B going into channel 2 of the X R5 is

$$V_{CH2} = V_{R_S} * \left[1 + \frac{R_{17}}{R_{16}}\right] = I_{PV} * R_S * A_o \tag{B.3}$$

where the gain

$$A_o = \left[1 + \frac{R_{17}}{R_{16}}\right]$$

The PV current is therefore obtained from

$$I_{PV} = \frac{V_{CH2}}{R_S}\left[\frac{1}{A_o}\right] = \frac{V_{CH2}}{0.1}\left[\frac{1}{11}\right] = \frac{V_{CH2}}{1.1} = 0.91 * V_{CH2} \quad \text{(B.4)}$$

The slope or multiplication factor is then 0.91.

References

Abdusalam, D., Mbamali, I., Mamman, M., Saleh, Y.M., 2012. An assessment of solar radiation patterns for sustainable implementation of Solar Home Systems in Nigeria. Am. Int. J. Contemp. Res. 2 (6), 238–243.

Ahmed, Z., Hussein, A.K., Sopian, K., 2017. Effect of dust on photovoltaic performance: review and research status. Latest Trends Renew. Energy Environ. Inform. < http://www.wseas.us/elibrary/conferences/2013/Malaysia/RESEN/RESEN-32.pdf > (2013) (accessed 12th August).

Babatunde, E.B., Akoshile, C.O., Falaiye, O.A., Willoughby, A.A., Ajibola, T.B., Adimula, I.A., Aro, T.O., 2009. Observation bio-effect of SW-global solar radiation in Ilorin in the tropics. Adv. Space Res. 43, 990–994.

Durán, E., Piliougine, M., Sidrach-de-Cardona, M., Galán, J., Andújar, J.M., 2008. Different methods to obtain the I-V curve of PV modules: a review. In: Proceedings of the 33rd IEEE Photovoltaic Specialists Conference (PVSC '08), San Diego, Calif., USA.

Garrigós, A., Blanes, J., 2005. Power MOSFET is Core of Regulated-DC Electronic Load, EDN, 92–93, March 17.

Gupta, V., 2017. Impact of dust deposition on solar photovoltaic panel in desert region. In: Review Conference Proceeding of 2nd International Conference on Engineering Technology, Science and Management Innovation (ICETSMI - at National Institute of Technical Teachers Training & Research (NITTTR). ISBN: 978 81- 932712-3-0.

Hamdaoui, M., Rabhi, A., El Hajjaji, A., Rahmoun, M., Azizi, M., 2009. Monitoring and control of the performances for photovoltaic systems. In: International Renewable Energy Congress. Sousse Tunisia.

Hemza, A., Abdeslam, H., Rachid, C., Pasquinelli, M., Barakel, D., 2015. Tracing current-voltage curve of solar panel Based on LabVIEW Arduino Interfacing. Bilişim Teknolojileri Dergisi, Cilt: 8, SAYI: 3, EYLÜL, 117–123.

Kaldellis, J.K., Fragos, P., Kapsali, M., 2011. Systematic experimental study of the pollution deposition impact on the energy yield of photovoltaic installations. Renew. Energy 36, 2717–2724.

Kopp, E.S., 2012. I-V Analysis Of Photovoltaic Modules Deployed Outdoors At Tucson Electric Power Solar Test Yard, M.Sc. Thesis. The University of Arizona.

Kuai, Y., Yuvarajan, S., 2006. An electronic load for testing photovoltaic panels. J. Power Sources 154, 308–313.

Leite, V., Chenlo, F., 2010. An improved electronic circuit for tracing the I-V characteristics of photovoltaic modules and strings. In: Proceedings of the International Conference on Renewable Energies PowerQuality, 23rd–25th March. Granada, Spain.

Leite, V., Batista, J., Chenlo, F., Afonso, J.L., 2012. Low-cost instrument for tracing current-voltage characteristics of photovoltaic modules. In: International Conference on Renewable Energies and Power Quality (ICREPQ'12), 28–30th March. Santiago de Compostela (Spain).

Mani, M., Pillai, R., 2010. Impact of dust on solar photovoltaic (PV) performance: research status, challenges and recommendations. Renew. Sustain. Energy Rev. 14, 3124–3131.

Ndiaye, A., Kébé, C.M.F., Ndiaye, P.A., Charki, A., Kobi, A., Sambou, V., 2013. Impact of dust on the photovoltaic (PV) modules characteristics after an exposition year in Sahelian environment: the case of Senegal. Int. J. Phys. Sci. 8 (21), 1166–1173.

Ojo, O., 1977. The Climates of West Africa. Heinneman, London, pp. 60–72.

Panwar, J.S., Mandliya, R., 2016. Analysis of I-V characteristics of photovoltaic modules using microcontroller based electronic loading arrangement. Int. J. Sci. Eng. Technol. Res. (IJSETR) 5, 1752–1754.

Park, R.S., Song, C.H., Han, K.M., Park, M.E., Lee, S.S., Kim, S.B., Shimizu, A., 2011. A study on the aerosol optical properties over East Asia using a combination of CMAQ-simulated aerosol optical properties and remote-sensing data via a data assimilation technique. Atmos. Chem. Phys 11, 12275–12296.

Papageorgasa, P., Piromalis, D., Valavanisa, T., Kambasisa, S., Iliopouloua, T., Vokasa, G., 2015. A low-cost and fast PV I-V curve tracer based on an open source platform with M2M communication capabilities for preventive monitoring. In: International Conference on Technologies and Materials for Renewable Energy, Environment and Sustainability. TMREES15. Energy Procedia, vol. 74, pp. 423–438.

Paudyal, B.A., Shakya, S.R., 2016. Dust accumulation effects on efficiency of solar PV modules for off grid purpose: a case study of Kathmandu. Sol. Energy 135, 103–110.

Ramaprabha, R., Jubair, S.H., Suhas, K., Lokesh, A., 2015. Design and implementation of efficient curve tracer for photovoltaic system under partial shaded conditions. Int. J. Electr. Eng. Inform. 7 (1), 140–149.

Renewable Energy Innovation [Online] < https://www.re-innovation.co.uk/docs/pv-i-v-curve-tracer > (accessed March 6, 2017).

Sulaiman, S.A., Hussain, H.H., Siti, N., Leh, N., Razali, M.S.I., 2011. Effects of dust on the performance of PV panels. World Acad. Sci., Eng. Technol. 58, 588–593.

Saidan, M., Albaali, A.G., Alasis, E., Kaldelis, J.K., 2016. Experimental study on the effect of dust deposition on solar photovoltaic panels in a desert environment. Renewable Energy 92, 499–505.

Sayyah, A., Horenstein, N., Mazumder, M.K., 2014. Energy yield loss caused by dust deposition on photovoltaic panels. Sol. Energy 107, 576–604.

Siddiqui, R., Bajpai, U., 2012. Correlation between thicknesses of dust collected on photovoltaic module and difference in efficiencies in composite climate. Int. J. Energy Environ. Eng. 3, 26. http://dx.doi.org/10.1186/2251-6832-3-26.

Tanesab, J., Parlevliet, D., Whale, J., Urmee, T., Pryor, T., 2015. The contribution of dust to performance degradation of PV modules in a temperate climate zone. Sol. Energy 130, 147–157.

Wang, C., Jeong, G.R., Mahowald, N., 2009. Particulate absorption of solar radiation: anthropogenic aerosols vs. dust. Atmos. Chem. Phys. 9, 3935–3945.

Willoughby, A.A., Omotosho, T.V., Aizebeokhai, A.P., 2014. A simple resistive load I-V curve tracer for monitoring photovoltaic module characteristics. In: The Fifth International Renewable Energy Congress, (IREC), Hammamet, Tunisia, 14-PVE-75-P978-1-4799-2195.

van Dyk, E.E., Gasheka, A.R., Meyer, E.L., 2002. Monitoring current-voltage characteristics of photovoltaic modules. In: Proceedings of the 29th IEEE Photovoltaic Specialists Conference, pp. 1516–1519.

Zimmermann, U., Edoff, M., 2012. A maximum power point tracker for long-term logging of PV module performance. IEEE J. Photovolt. 2 (1), 47–55.